Vacuum 101 (2014) 250–256

Contents lists available at ScienceDirect

Vacuum

journal homepage: www.elsevier.com/locate/vacuum

The effects of thickness on the electrical, optical, structural and morphological properties of Al and Ga co-doped ZnO films grown by linear facing target sputtering

Ki-Won Seo [a], Hyun-Su Shin [a], Ju-Hyun Lee [a], Kwon-Bum Chung [b], Han-Ki Kim [a, *]

[a] Department of Advanced Materials Engineering for Information and Electronics, Kyung Hee University, 1 Seocheon-dong, Yongin-si, Gyeonggi-do 446-701, South Korea

[b] Department of Physics, Dankook University, Mt. 29, Anseo-Dong, Chenan 330-714, South Korea

ARTICLE INFO

Article history:
Received 7 August 2013
Received in revised form
6 September 2013
Accepted 8 September 2013

Keywords:
Al and Ga co-doped ZnO
Thickness
Linear facing target sputtering

ABSTRACT

We investigated the effects of thickness on the electrical, optical, structural, and morphological properties of Al and Ga co-doped ZnO films (AGZO) grown by linear facing target sputtering (LFTS) for use as a transparent contact layer (TCL) in GaN-light emitting diodes (LEDs). Below a critical thickness of 200 nm, the resistivity and optical transmittance of the AGZO films were significantly affected by the thickness of the AGZO films. However, above a thickness of 200 nm, the AGZO films had similar resistivities and optical transmittances due to the stable columnar structure, which developed at a thickness of 200 nm. Due to the change of the growth mode with increasing thickness, the microstructure and surface morphology were also affected by the film thickness. Based on the figure of merit values, we determined that the optimized thickness of the LFTS-grown AGZO film was 200 nm, which was applied in a GaN-LED as a TCL. Successful operation of GaN-LEDs with an optimized AGZO film without plasma damage indicates that the LFTS-grown AGZO film is promising plasma damage-free TCL for use in GaN-LEDs.

1. Introduction

ZnO-based transparent conducting oxide (TCO) films are highly degenerate wide bandgap semiconductors with a high conductivity and optical transmittance in the visible wavelength region [1]. Although Sn-doped In_2O_3 (ITO) has been widely used as TCO films in flat panel displays, photovoltaics, touch screen panels, and GaN-light emitting diodes (LEDs), the development of ZnO-based indium-free TCO as a substitute for ITO is imperative, due to limited availability and rapidly increasing cost of indium [2–4]. As a promising candidate as a substitute for ITO film, both Al-doped ZnO (AZO) and Ga-doped ZnO (GZO) films have been extensively investigated because they have a low resistivity and high transparency comparable to conventional ITO films [5–8]. Recently, Al and Ga co-doped ZnO (AGZO) films prepared by AZO and GZO co-sputtering have been suggested as ZnO-based TCO films. To improve the stability of AZO films, AZO and GZO mixed films has been investigated. Kang et al. reported that a co-sputtered AGZO film had a resistivity of 2.4×10^{-3} Ohm-cm and an optical transmittance between 77 and 90% in the visible wavelength region [9]. Lin et al. also reported that an AGZO film grown by pulsed direct current magnetron sputtering had a low resistivity of 8.2×10^{-4} Ohm-cm and an average transmittance above 80% [10]. Although the electrical and optical properties of co-sputtered AGZO films have been investigated, the effects of the film thickness on the electrical, optical, structural, and morphological properties of AGZO films grown by linear facing target sputtering (LFTS) have not been reported. Because the thickness of an AGZO film critically affects the sheet resistance and optical transmittance like other TCO films such as ITO, IZTO, AZO, and GZO, determination of optimized thickness for the LFTS-grown AGZO TCL layer is very important [11–15]. In addition, to fabricate a sputtered-transparent conducting layer (TCL) in the GaN-light emitting diodes (LEDs), exact understanding of damage free mechanism for AZO and GZO co-sputtered films is necessary because conventional sputtering process led to a severe degradation of p-GaN layer. Bombardment of energetic particles onto p-GaN during sputtering process resulted in compensation of p-GaN layer and degraded the electrical properties of p-GaN layer. For those reasons, there have been no reports of the sputtered AGZO films as a TCL in the GaN-LEDs.

In this work, we investigated the dependencies of the electrical, optical, structural, and morphological properties on the thickness

* Corresponding author. Tel.: +82 31 201 2462.
E-mail address: imdlhkkim@khu.ac.kr (H.-K. Kim).

0042-207X/$ – see front matter © 2013 Elsevier Ltd. All rights reserved.
http://dx.doi.org/10.1016/j.vacuum.2013.09.009

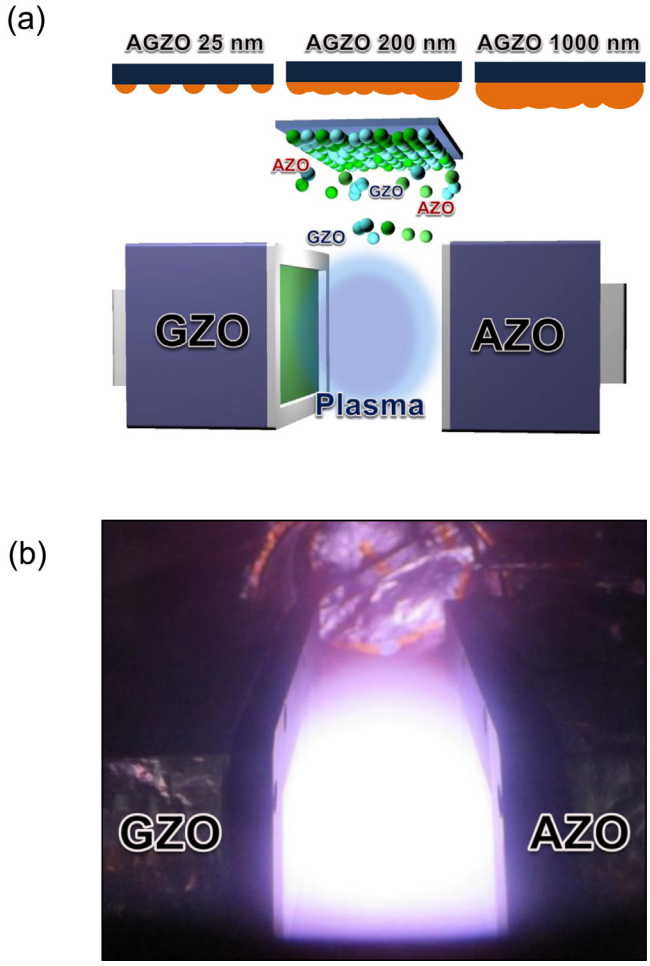

Fig. 1. (a) Schematics of the linear facing target sputtering system with rotating facing guns equipped with AZO and GZO hetero targets. The upper panels show a schematic of the AGZO films with different thicknesses grown by LFTS. (b) The argon plasma formed between the AZO and GZO targets was effectively confined high density plasma.

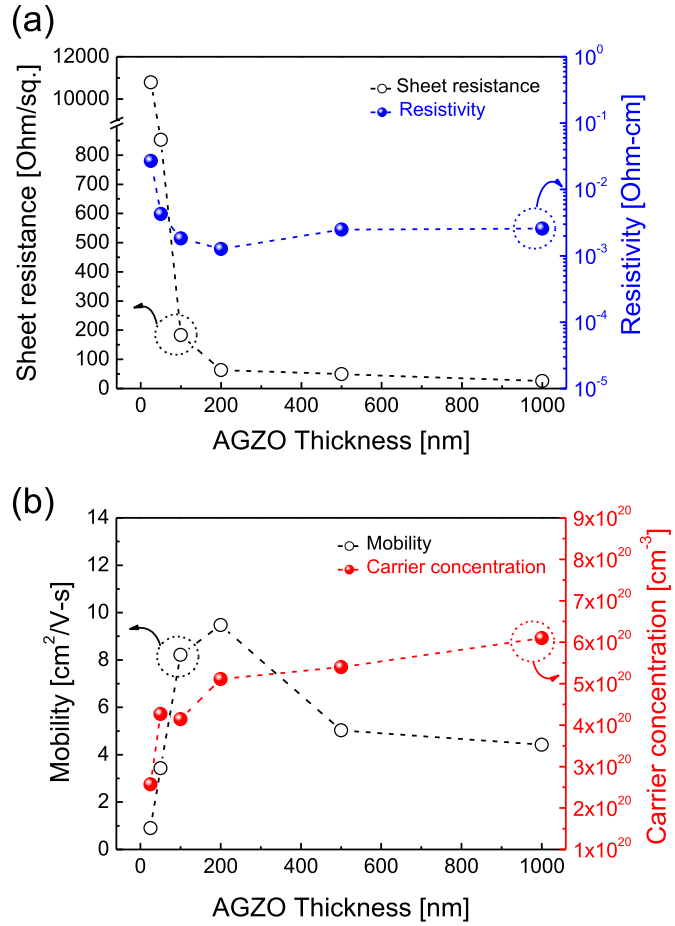

Fig. 2. (a) Sheet resistance, resistivity, (b) carrier mobility, and concentration of the AGZO electrodes as a function of thickness.

of AGZO films grown by an LFTS system using Al–Zn–O (AZO) and Ga–Zn–O (GZO) co-sputtering. Based on the figure of merit values, we optimized the thickness of the AGZO film for application in GaN-LEDs as a plasma damage-free TCL. In addition, we compared the performance of GaN-LEDs with LFTS-grown AGZO TCL and conventional DC sputtered AGZO TCL.

2. Experimental section

Al and Ga co-doped ZnO films were prepared on glass substrate with different thicknesses (25, 50, 100, 200, 500, and 1000 nm) by using an LFTS system equipped with rotatable facing cathodes at room temperature by increasing the sputtering time. Using commercial AZO (3 wt % Al-doped ZnO: Heesung Metal Ltd) and GZO (3 wt % Ga-doped ZnO: Advanced Nano Products) targets, AGZO films were co-sputtered in the LFTS system, in which the AZO and GZO targets were parallel and faced each other at a TTD of 650 mm. Fig. 1(a) shows a schematic diagram of the LFTS used to prepare the AGZO films on glass substrates without plasma damage. A detailed description of the LFTS system was given in our previous works [16–18]. As shown in Fig. 1(a), the negatively applied voltage to both AZO and GZO targets and one-directional magnet fields from the AZO to the GZO target led to the effective confinement of the plasma between the AZO and GZO targets. The oscillating motion of electrons in the confined plasma creates high density plasma between the AZO and GZO targets, as we previously reported [18]. Fig. 1(b) shows a picture of the high density plasma, which is confined between the AZO and GZO targets. The AGZO films were co-sputtered on glass substrates with dimensions of 25 × 25 mm^2 at a constant Ar flow ratio of 20 sccm and a working pressure of 0.3 mTorr as a function of the AGZO thickness which ranged from 25 to 1000 nm. A constant DC power of 250 W was simultaneously applied to both the AZO and GZO targets. The thickness of the AGZO films was controlled by adjusting the sputtering time. After co-sputtering of the AZO and GZO targets, all AGZO films were rapidly thermal-annealed at 600 °C for 1 min under H_2 ambient to activate Al and Ga dopants and improve the crystallinity [19]. The thickness of the AGZO films was measured by a surface profilometer (NANOMAP-LS). The electrical and optical properties of the AGZO films were analyzed by Hall measurements (HL5500PC, Accent Optical Technology) and a UV/visible spectrometer (UV 540, Unicam) at room temperature as a function of the AGZO thickness. The refractive index of the AGZO films was measured by a spectroscopic ellipsometer (J.A. Woollam, VASE) as a function of the film thickness. The structural properties of the AGZO films were analyzed by X-ray diffraction (XRD: M18XHF-SRA) using a standard θ-2θ geometry diffractometer with Cu–K$_\alpha$ radiation (1.54 Å) as a function of the AGZO thickness. In addition, the surface morphology of the AGZO films was investigated by using a field emission scanning electron microscope (FESEM: LEO SUPRA 55).

The root-mean-square (RMS) roughness and topography of the AGZO films were analyzed by atomic force microscopy (AFM: PUCOStation STD). To investigate the feasibility of applying the optimized AGZO film as a TCL for GaN-LEDs, we fabricated top-emission LEDs with a size of 300 × 600 μm^2. The AGZO TCL with a thickness of 200 nm was partially wet etched in a dilute HCL solution. Then, the LED structure was fabricated by dry-etching of n-GaN using inductively coupled plasma with $CH_4/Cl_2/H_2/Ar$ gas sources. Finally, a Cr/Au (30/100 nm) layer was deposited as the p- and n- electrodes. To compare the performances of GaN-LEDs with AGZO TCL prepared by different sputtering method, we prepared 200 nm thick AGZO TCL layer prepared by conventional DC sputtering with tiled multi-cathodes.

3. Results and discussion

The sheet resistance and resistivity of the 600 °C-annealed AGZO films as a function of thickness are shown in Fig. 2(a). The sheet resistance of the AGZO films significantly decreased as the AGZO film thickness was increased. At a thickness of 1000 nm, the AGZO films exhibited the lowest sheet resistance of 25.7 Ohm/square. It is noteworthy that the sheet resistance of the AGZO films decreased rapidly with increasing film thickness in the 25–200 nm range due to the rapid decrease of resistivity. However, above a thickness of 200 nm, the AGZO film exhibited a similar resistivity between 1.3 × 10^{-3} and 2.5 × 10^{-3} Ohm-cm, regardless of the film thickness. A similar resistivity dependence on the thickness was also reported for ITO films [13,14]. As discussed by Kim et al., thicker ITO films showed lower resistivities because the grain size and grain boundary of ITO films are critically affected by the film thickness [13]. In the thickness region below 100 nm, the resistivity of the ITO films decreased rapidly due to increased grain size and improved discontinuities, while ITO films with thicknesses above 350 nm showed a fairly constant resistivity due to their constant mobility and carrier density. Wang et al. and Lin et al. also reported that resistivity of Al-doped ZnO and Ti-doped ZnO films was critically affected by film thickness [20,21]. Like ITO and ZnO-based films, the dependence of the resistivity of AGZO films on thickness can be attributed to the change of the grain size and grain boundary density with increasing thickness, as demonstrated in the XRD results shown in Fig. 5 [14,15,22]. In addition, activation of Al and Ga dopant in ZnO matrix also affected the electrical properties of the AGZO films. Fig. 2(b) shows the carrier mobility and concentration of the AGZO films as a function of the film thickness. In the thin thickness region below 200 nm, the carrier mobility of the AGZO film rapidly increased from 0.9 cm^2/V-s to 9.5 cm^2/V-s with increasing thickness, which is the main reason for the decreased resistivity of the thin AGZO films. Above a thickness of 200 nm, the carrier mobility of the AGZO film decreased slightly from 9.5 cm^2/V-s to 4.42 cm^2/V-s with increasing thickness. The decreased mobility of the AGZO film could be attributed to the increased carrier concentration which led to the severe electron–electron scattering [23]. The decreased mobility resulted in an increase of the resistivity above a thickness of 500 nm, as shown in Fig. 2(a). However, with increasing thickness, the carrier concentration also increased from 2.5 × 10^{20} and 6.0 × 10^{20} cm^{-3}, indicating the effective activation of Al and Ga dopant in the thicker AGZO films. In general, activation of Al and Ga dopant in AGZO films occurred by breaking Al–O and Ga–O bonds and substitution of activated Al and Ga dopant with Zn sites. The increased carrier concentration of the AGZO films with increasing thickness indicated that the activation of Al and Ga dopant in thicker AGZO films is more favorable than very thin AGZO films. Due to this high carrier concentration, the thick AGZO film above 200 nm showed fairly low resistivity, even though they showed decreased carrier mobility.

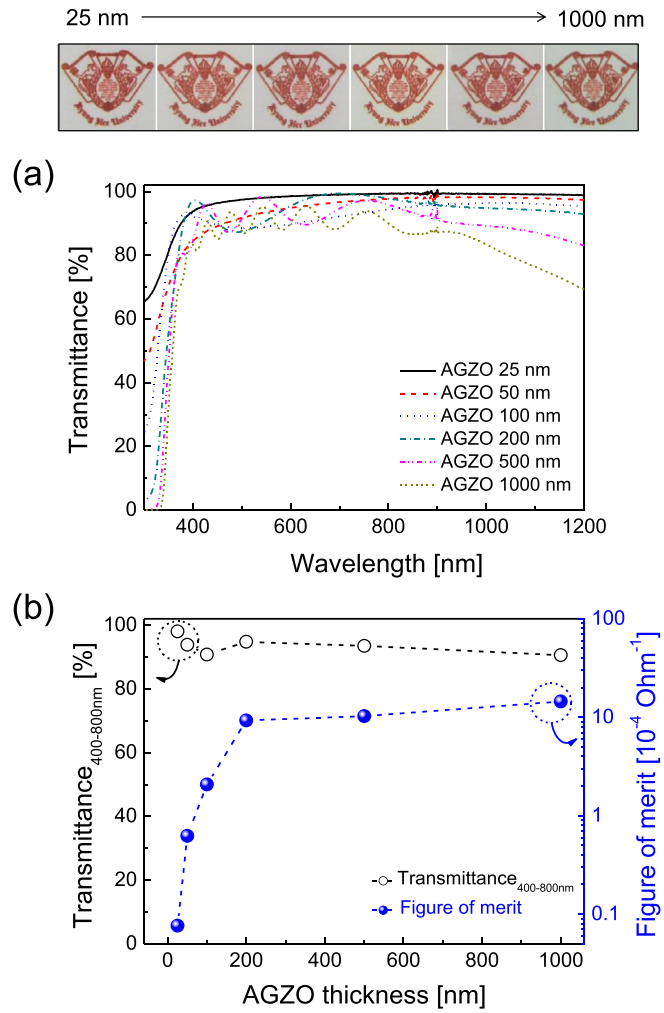

Fig. 3. (a) Optical transmittance of the LFTS-grown AGZO film as a function of thickness. The upper panels show the optical transparency of the AGZO films grown at different thicknesses on a Kyung Hee University seal. (b) Figure of merit values calculated from the sheet resistance and average optical transmittance obtained between wavelengths of 400 and 800 nm.

Therefore, the decreased resistivity of the AGZO films with increasing thickness was mainly affected by the change of the carrier mobility of the AGZO films.

Fig. 3(a) shows the optical transmittance of the LFTS-grown AGZO films fabricated under constant deposition conditions as a function of the film thickness. The upper panel shows pictures of the AGZO samples on a Kyung Hee University seal with high transparency. Regardless of the film thickness, all AGZO films showed a very high optical transparency. As can be seen in Fig. 3(a), as the AGZO film thickness increases, the optical transmittance varied due to interference phenomena. All AGZO films showed a fairly high average optical transmittance in the visible wavelength range. In the case of the average optical transmittance between 400 and 800 nm, the AGZO film with a thickness of 200 nm showed the highest optical transmittance of 94.8%. However, for wavelengths above 900 nm in the near infrared (NIR) range, the transmittance of the 500 and 1000 nm thick AGZO films abruptly decreased due to free carrier absorption. Due to the shift of the plasma wavelength (λ_p), the thicker AGZO film exhibited a lower NIR transmittance [24]. To determine the optimum thickness for deposition of the AGZO films, the figure of merit value, which is defined as $\phi_{TC} = T^{10}/R_{sh}$, was calculated using the sheet resistance (R_{sh}) and average

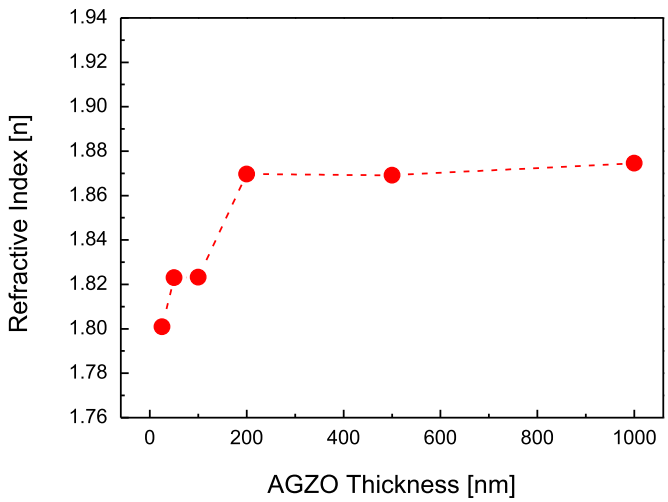

Fig. 4. Refractive index (n) as a function of the AGZO film thickness.

transmittance (T) of the AGZO films [25]. Fig. 3(b) shows the calculated ϕ_{TC} values and average optical transmittances of the LFTS-grown AGZO films as a function of thickness. For thin AGZO films below 200 nm, the ϕ_{TC} value abruptly increased while the ϕ_{TC} values of the thicker AGZO films (>200 nm) were fairly constant, due to the effect of the thickness of the AGZO films on the sheet resistance as shown in Fig. 2(a). The AGZO film with a thickness of 200 nm showed high ϕ_{TC} value due to the highest optical transmittance of 94.8% and low sheet resistance of 63.2 Ohm/square. Therefore, we determined that the optimized thickness of AGZO film is 200 nm for application in GaN-based LEDs as a TCL.

Fig. 4 shows the refractive index (n) of the AGZO films as a function of the film thickness obtained by measuring the SE at 550 nm wavelength. Below a thickness of 200 nm, the refractive index (n) increased with increasing AGZO thickness. Above a thickness of 200 nm, the n values of the AGZO films were approximately constant. The refractive index of an oxide film can be correlated to the film density and composition of the film [26]. Therefore, the density of the AGZO film continuously increased up to a thickness of 200 nm, and then was saturated above a thickness of 200 nm. These tendencies of the film density affect the electrical and optical properties of AGZO films because a lower film density can cause more scattering effects of electrons and light inside the films.

To investigate the thickness effect on the microstructure of the LFTS-grown AGZO films, XRD analysis was performed. Fig. 5(a) shows the XRD plots obtained from the LFTS-grown AGZO films as a function of thickness. All of the LFTS-grown AGZO films are highly oriented with the c-axis perpendicular to the glass substrate except for the 25 nm thick AGZO film, as in the case of conventional batch type sputter-grown AGZO films [10]. The 50 nm thick AGZO film had a strong (002) peak at $2\theta = 34.4°$ indicating that the LFTS-grown AGZO films have a well-developed Wurtzite structure with a strongly (002) preferred orientation. With increasing thickness, the intensity of the (002) peak also significantly increased due to the preferred orientation of the AGZO grains along the [002] direction. Although there is an additional weak (101) peak in the 1000 nm thick AGZO film, the increased film thickness mainly affected the (002) preferred orientation in the AGZO columnar structure. Fig. 5(b) shows the variation of the full-width at half maximum (FWHM) of the (002) and the calculated (002) grain size as a function of thickness. The grain size was calculated from the XRD pattern using Scherrer's formula,

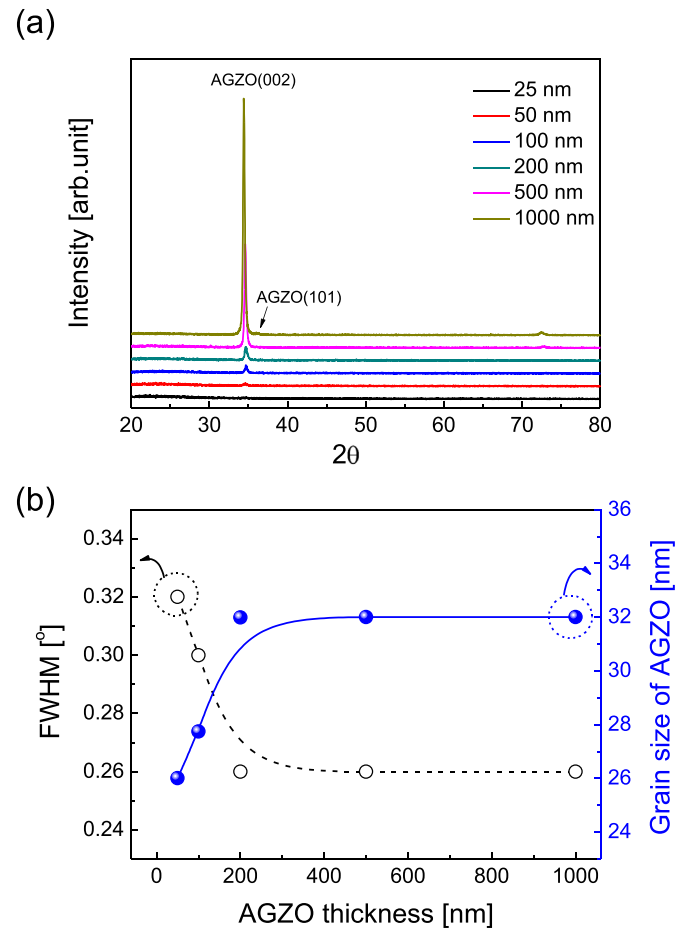

Fig. 5. (a) XRD plots of the LFTS-grown AGZO films as a function of thickness. (b) The FWHM variation of the XRD plot and the grain size calculated by the Scherrer formula. All of the AGZO films were rapidly thermal-annealed at 600 °C for 1 min under H_2 ambient.

$$D = 0.9\frac{\lambda}{\beta\cos\theta}$$

where D is the grain size of the AGZO films, λ is the wavelength of the X-rays (Cu K_α 1.54056 Å), β is the broadening of the diffraction line measured at half its maximum intensity in radians (FWHM), and θ is the diffractive angle [27]. With increasing thickness from 25 to 200 nm, the (002) oriented grain size increased abruptly. However, it can be seen that in the films with thicknesses greater than 200 nm is independent of the thickness. This trend corresponds to the refractive index and film density result in Fig. 4.

The dependence of the surface morphology of the LFTS-grown AGZO films on the film thickness was investigated by FESEM. Fig. 6 shows surface and cross-sectional FESEM images of the 50, 200, and 1000 nm thick AGZO films. As expected from the XRD results, the grain size of the LFTS-grown AGZO films increased gradually with increasing thickness. The 50 nm thick AGZO film shown in Fig. 6(a) and (b) has very small grains. A further increase of the film thickness led to increased sizes of the grains of the AGZO films, as shown in Fig. 6(e) and (f). With increasing thickness, a rough surface morphology developed due to the (002) texture evolution of Wurtzite structured AGZO films. Fig. 7 shows AFM surface images and the RMS roughness of the LFTS-grown AGZO films as a function of the AGZO thickness. The surface morphology of the AGZO films changed with increasing AGZO thickness. The RMS roughness values of the 25, 50, 100, 200, 500, and 1000 nm

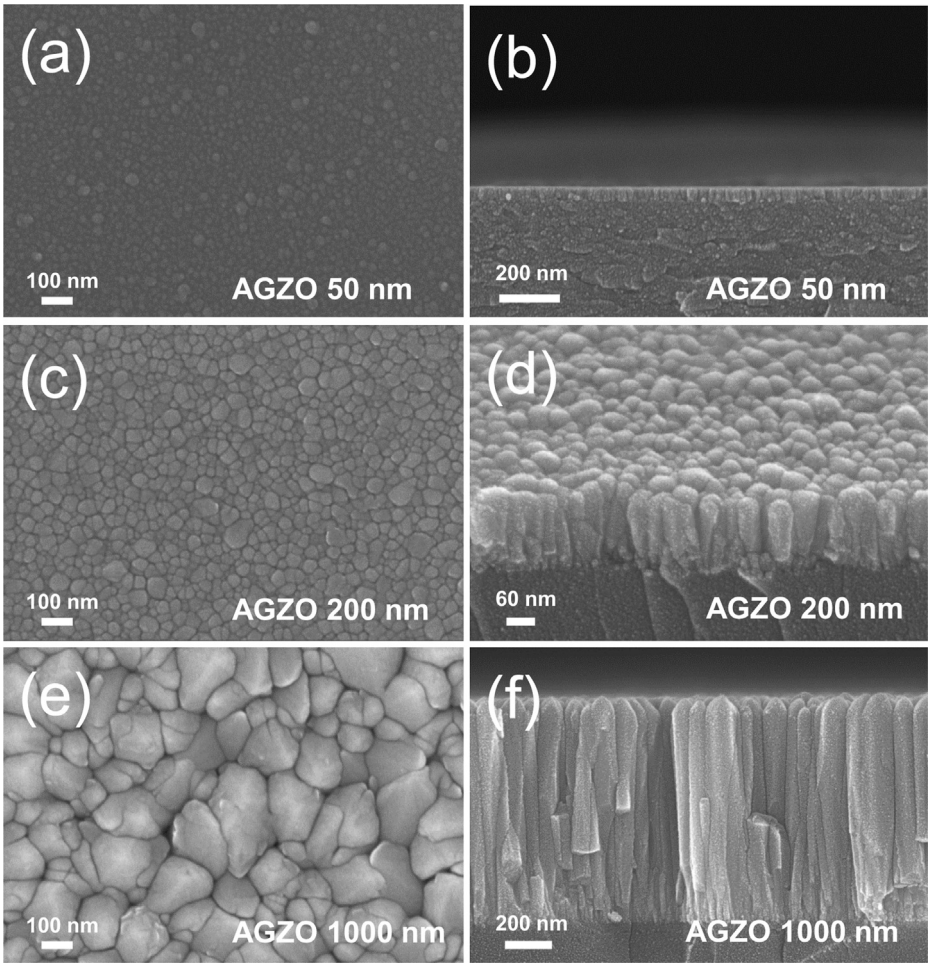

Fig. 6. Surface and cross-sectional FESEM images of AGZO films with thicknesses of 50 nm ((a) and (b)), 200 nm ((c) and (d)) and 1000 nm ((e) and (f)), respectively.

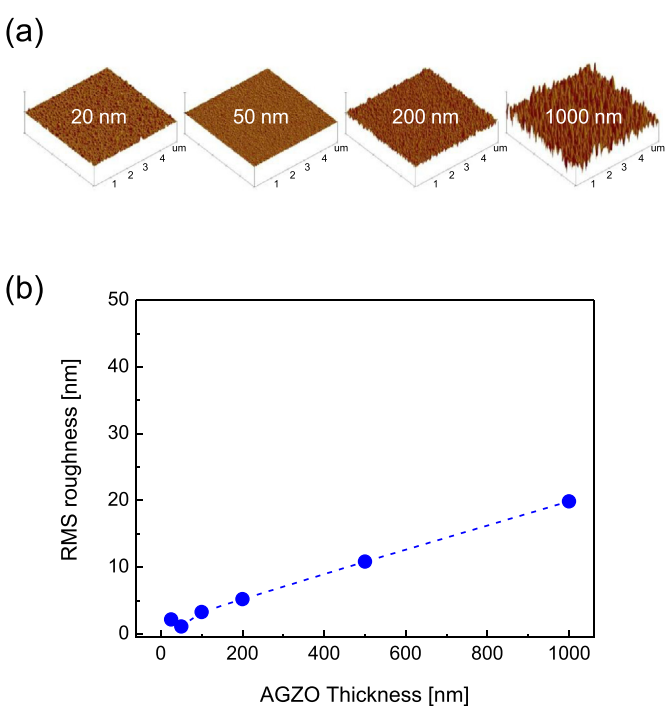

Fig. 7. (a) Surface AFM images of AGZO films with various AGZO thicknesses. (b) RMS roughnesses of the AGZO films as a function of the AGZO film thickness.

thick AGZO films were 2.2, 1.1, 3.3, 5.2, 10.8, and 19.8 nm, respectively. With increasing thickness, the RMS roughness of the AGZO films increased, due to the formation of a textured surface with a pyramid shape, as shown in Fig. 6.

Based on the figure of merit values of the AGZO films, we determined that the optimum AGZO thickness is 200 nm for application in GaN-LEDs as a promising TCL. Fig. 8(a) shows a schematic diagram of the process used to fabricate the GaN-LED with the LFTS-grown AGZO TCL. Fig. 8(b) shows the *I*–*V* characteristics of the LFTS-grown AGZO contact on p-GaN as a function of the RTA temperature. It is evident that an increased RTA temperature led to an improvement of the *I*–*V* behavior of the 200 nm thick AGZO contact on p-GaN. Below an RTA temperature of 500 °C, the AGZO contact revealed rectifying *I*–*V* behavior. However, an increase of the RTA temperature to 600 °C resulted in linear *I*–*V* characteristics, indicating the formation of an AGZO ohmic contact on the p-GaN layer. The specific contact resistances were calculated from plots of the measured resistances versus the spacings between the circular transmission line method (c-TLM) pads. The specific contact resistance of the 600 °C annealed AGZO contact was determined to be 2.7×10^{-3} ohm-cm [2]. Even though the AGZO film was grown by a sputtering process, the AGZO contact resulted in linear *I*–*V* characteristics and the formation of ohmic contact without severe plasma damage, because the LFTS process reduced the direct plasma irradiation on p-GaN during the AGZO sputtering process as we previously reported [16–18]. Fig. 8(c) shows the *I*–*V* characteristics of the GaN-LED with the 200 nm thick AGZO TCL prepared by LFTS and conventional DC

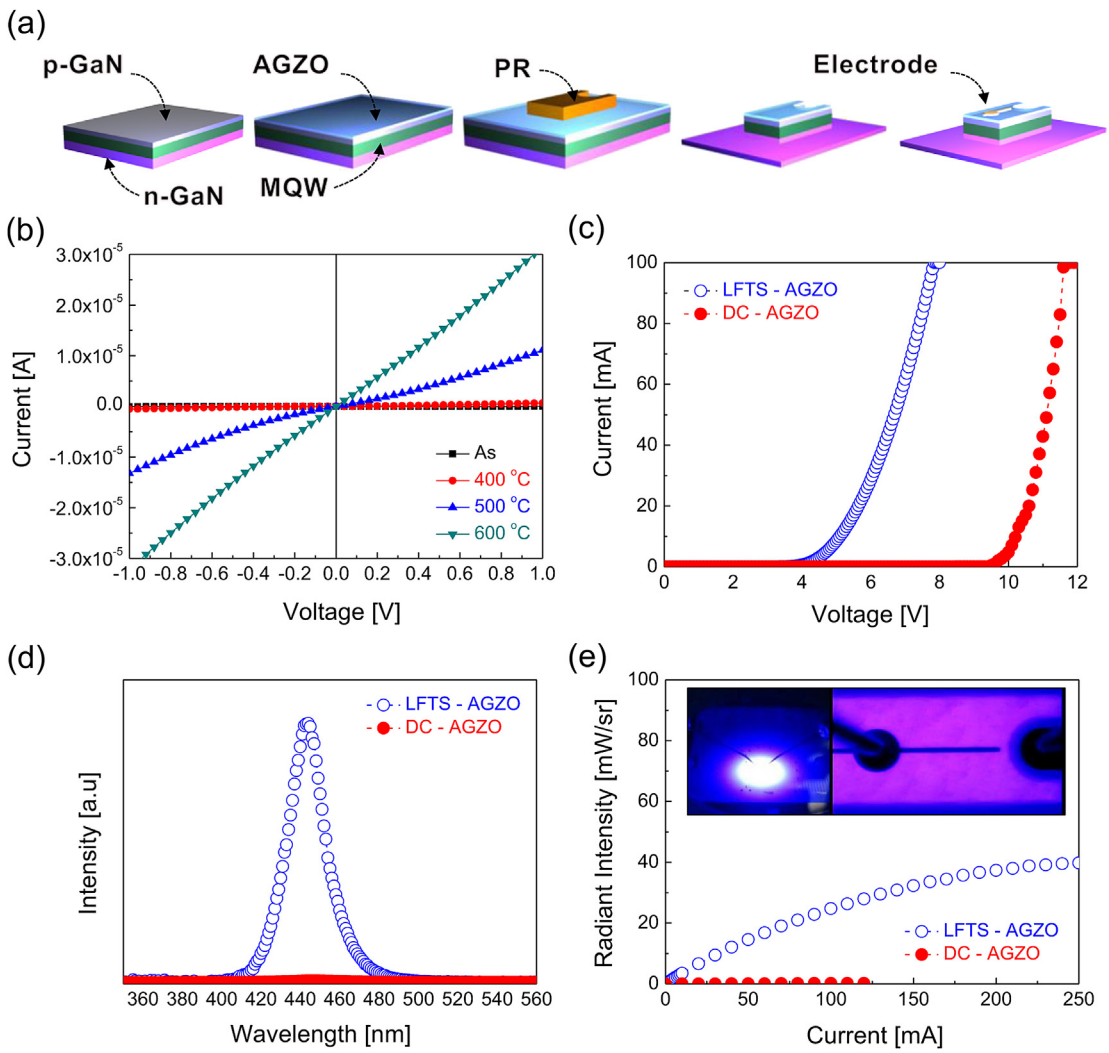

Fig. 8. (a) Schematic diagram of the GaN-LED fabrication process with the AGZO TCL. (b) *I–V* characteristics of the LFTS AGZO contact on p-GaN as a function of the RTA temperature. (c) *I–V* characteristics and (d) electroluminescence spectra of GaN-LEDs with the AGZO TCL prepared by LFTS and conventional DC sputtering. (e) Dependence of the radiant intensity on the injection current of the GaN-LED with the AGZO TCL layer prepared by LFTS and conventional DC sputtering.

sputtering. It can be seen that the GaN-LED with the LFTS-grown AGZO TCL showed a much lower turn on voltage of 5 V, indicating plasma damage free sputtering of LFTS. However, the GaN-LED with LFTS-grown AGZO TCL showed fairly high turn on voltage of ~5 V, due to the high series resistance of the AGZO TCL along the path of current spreading from the p-pad electrode, than a conventional ITO TCL grown by evaporation. Further optimization of AGZO films could reduce the turn on voltage of GaN-LEDs because series resistance is closely related with resistivity of the AGZO TCL. Fig. 8(d) shows the electroluminescence (EL) spectrum of the GaN-LED with LFTS-grown and DC sputtered AGZO TCL with a thickness of 200 nm. As expected from the *I–V* characteristics, the GaN-LED showed high luminescence intensity. In Fig. 8(e), the radiant intensity of the GaN-LED with the AGZO TCL with a thickness of 200 nm was 7 mW/sr at 20 mA where the inset shows the blue emission from the GaN-LEDs. Fig. 8(d)–(e) shows that the GaN-LED with the LFTS-grown AGZO TCL successfully operated without severe plasma damage even though the AGZO TCL was grown by a sputtering process. However, further process optimization of GaN-LEDs with AGZO TCL in order to increase the efficiency and decrease the turn on voltage is necessary to improve the performance of the GaN-LEDs. Successful fabrication and operation of GaN-LEDs with an AGZO TCL without plasma damage suggests that the LFTS-grown AGZO film is promising plasma damage-free TCL for application in GaN-LEDs.

4. Conclusions

We investigated the dependencies of the electrical, optical, structural, and morphological properties on the thickness of AGZO films grown by an LFTS system for application in high-performance GaN-LEDs. Effective confinement of high density plasma between the AZO and GZO targets led to the sputtering of AGZO TCL on the p-GaN layer without plasma damage. The resistivity of the AGZO films decreased in the thin thickness region below 200 nm and then became saturated due to the saturated grain size. However, the average transmittance in the visible region was fairly high, regardless of the AGZO thickness. With an optimized AGZO thickness of 200 nm, we obtained a sheet resistance of 63.2 Ohm/square, an average transmittance of 94.8% in the visible range, an RMS roughness of 5.2 nm, and a figure of merit value of 9.3×10^{-4} Ohm^{-1} without plasma damage, which are applicable in GaN-LEDs as a TCL. Moreover, the successful operation of GaN-LED with an LFTS-grown AGZO TCL with a thickness of 200 nm indicate

that LFTS-grown AGZO film is a promising plasma damage-free TCL for GaN-based LEDs.

Acknowledgments

This work was supported by the Industrial Core Technology Development Programs of the Korea Ministry of Knowledge Economy (10033573) and in part by Basic Science Research Program through the National Research Foundation of Korea (NRF) funded by the Ministry of Education, Science and Technology (2012-0002430).

References

[1] Ellmer K, Klein A, Rech B. Transpar Conduct Zinc Oxide 2008.
[2] Ray S, Banerjee R, Basu N, Batabyal AK, Barua AK. J Appl Phys 1983;54:3497.
[3] Tahar RBH, Ban T, Ohya Y, Takahashi Y. J Appl Phys 1998;83:2631.
[4] Chipman Andrea. Nature 2007;449:131.
[5] Bhosle V, Tiwari A, Narayan J. Appl Phys Lett 2006;88:032106.
[6] Bhosle V, Narayan J. J Appl Phys 2006;100:093519.
[7] Gomez H, de la L. Olvera M. Mater Sci Eng B 2006;134:20.
[8] Berry JJ, Ginley DS, Burrow PE. Appl Phys Lett 2008;92:193304.
[9] Kang J, Kim HW, Lee C. J Korean Phys Soc 2010;56:576.
[10] Lin YC, Chen TY, Wang LC, Lien SY. J Electrochem Soc 2012;159:H599.
[11] Kim H-K, Ahn K-J, Jang H-K, Lee H-S. J Electrochem Soc 2012;159:H38.
[12] Choi K-H, Jeong J-A, Kim H-K. Sol Energy Mater Sol Cells 2010;94:1822.
[13] Kim H, Horwits JS, Kushto G, Pique A, Kafafi ZH, Gilmore CM, et al. J Appl Phys 2000;88:6021.
[14] Hao L, Diao X, Xu H, Gu B, Wang T. Appl Surf Sci 2008;254:3504.
[15] Hao X, Ma J, Zhang D, Yang T, Ma H, Yang Y, et al. Appl Surf Sci 2001;183:137.
[16] Nakagawa S, Mizuno K, Naoe M. J Appl Phys 2003;93:8170.
[17] Jeong J-A, Shin H-S, Choi K-H, Kim H-K. J Phys D Appl Phys 2010;43:J465403.
[18] Shin H-S, Lee J-H, Kim H-K. J Vac Sci Technol A 2012;30:031510–1.
[19] Jeong M-C, Oh B-Y, Ham M-H, Myoung J-M. Appl Phys Lett 2006;88:202105.
[20] Wang F, Wu MZ, Wang YY, Yu YM, Wu XM, Zhuge LJ. Vacuum 2013;89:127.
[21] Lin S-S, Huang J-L, Lii D-F. Surf Coat Technol 2005;190:372.
[22] Kim H, Horwitz JS, Kushto G, Pique A, Kafafi ZH. J Appl Phys 2000;88:6021.
[23] Hilsum C. Electron Lett 1974;10:259.
[24] Wooten F. Optical properties of solids. New York: Academic Press; 1972.
[25] Haacke G. J Appl Phys 1976;47:4086.
[26] Kim J-H, Chung C-O, Sheen D, Sohn Y-S, Sohn H-C, Kim J-W, et al. J Appl Phys 2004;96:1435.
[27] Cullity BD. Elements of X-ray diffraction. USA: Addison-Wesley; 1978.